Civelekoglu-Scholey et al., http://www.jcb.org/cgi/content/full/jcb.201301022/DC1

THE JOURNAL OF CELL BIOLOGY

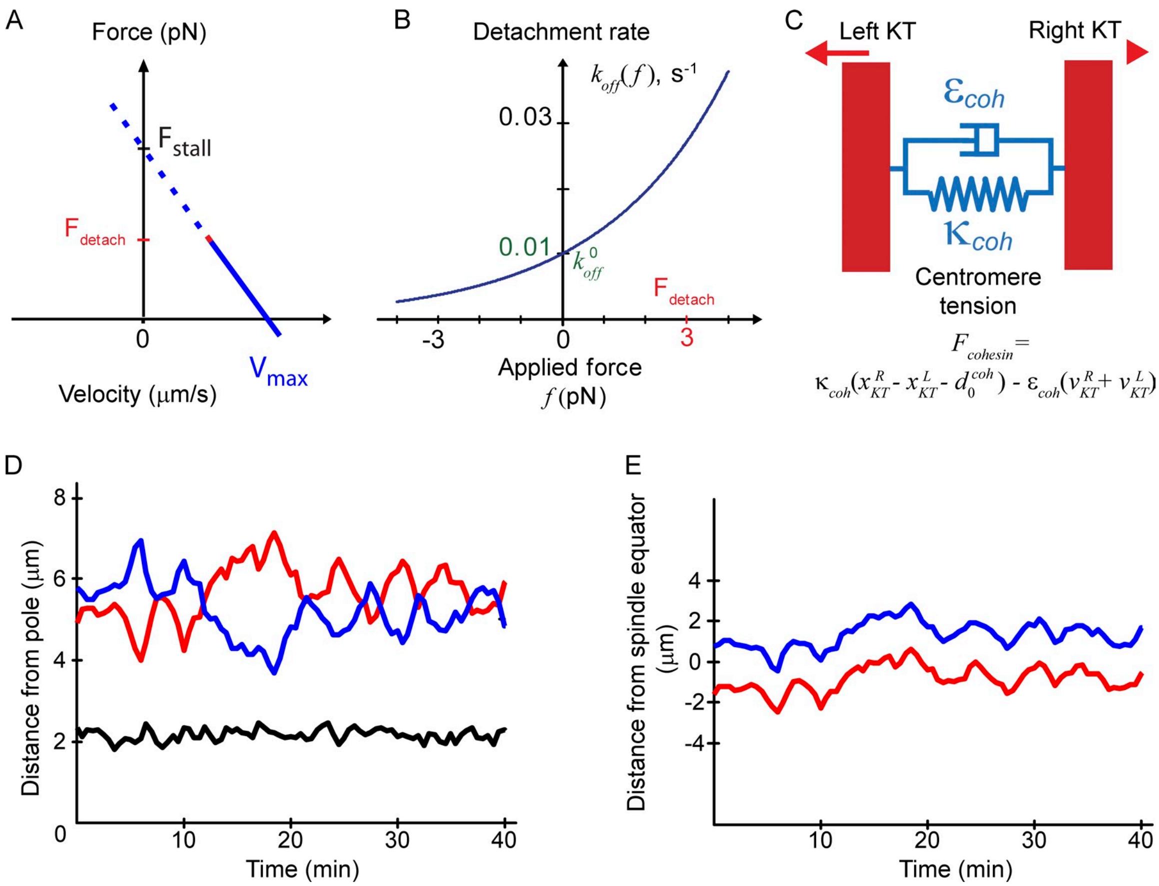

Figure S1. **Biophysical properties of motors and nonmotor proteins, and behavior of sister KTs in the model with motor-dependent KT–MT interactions.** (A) Typical form of the motor protein force–velocity relationship. (B) Force-sensitive dissociation rate of motors and nonmotor proteins. (C) Description of the tension force exerted on the KTs by viscoelastic cohesin bonds. (D) Distance of a pair of middle sister KTs (left KT in red, right KT in blue) from the spindle pole and inter-KT distance (black) over time. (E) Distance of sister KTs (same pair shown in D) from the spindle equator, over time.

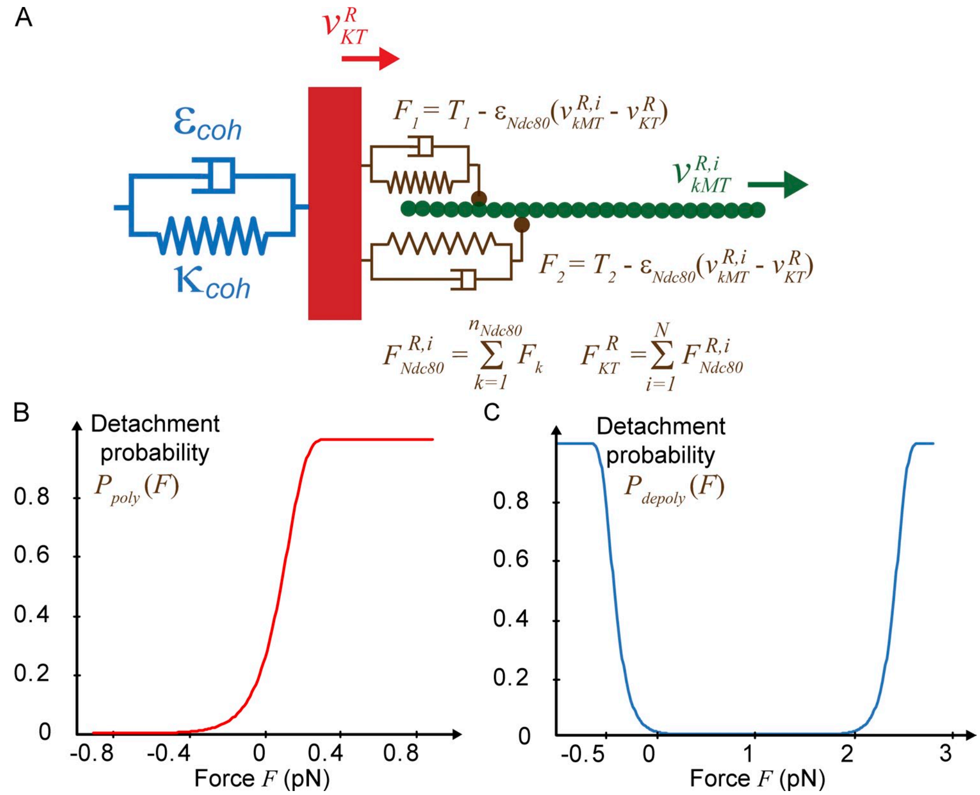

Figure S2. **Tension forces exerted on the KT and the kMTs by MT-bound Ndc80 complexes and force-sensitive dissociation kinetics of the Ndc80 complex.** (A) Total tension force exerted by multiple bound Ndc80 complexes (brown mechanical elements) on the KT (red bar) and the kMT (green rod). Only a single right KT-attached MT is depicted for simplicity. The cohesin between the sister KTs is shown (blue mechanical element), but the left KT is not depicted. (B) The Ndc80 complex dissociation rate from polymerizing MTs increases with increased load. (C) Ndc80 complex dissociation rate from depolymerizing MTs is biphasic: it initially decreases with increasing load (near zero), then increases with further increased load.

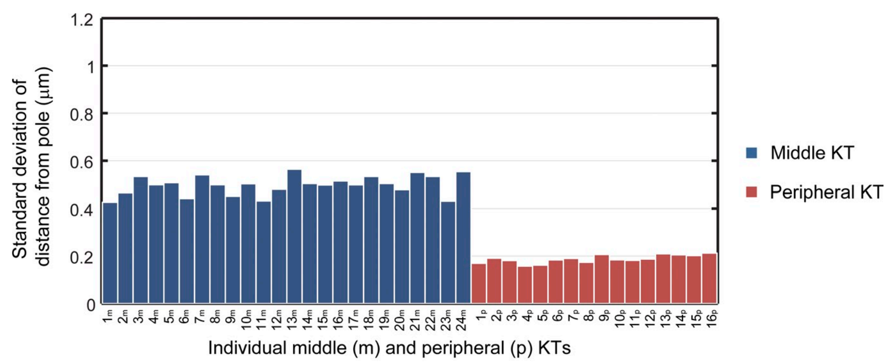

Figure S3. **Distribution of the standard deviations of the distances from the pole for middle (blue) and peripheral (red) KTs produced by the model.** Note, both the actual values and the variability of the standard deviations are smaller compared with the experimental data (Fig. 1 D) because of the higher accuracy of the simulation data. However, the mean inter-KT distances (Fig. 5 C) do not differ between experimental and modeling data.

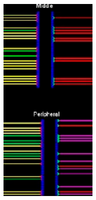

Video 1. **KT and kMT dynamics for oscillating and nonoscillating sister KT pairs in the model.** The solutions of the equations, plotted in the form of a movie, illustrate the attachment and detachment of KTs to growing/shrinking and poleward fluxing MTs for the middle oscillating (top) and peripheral nonoscillating (bottom) sister KT pairs. The position of the KT inner plate is shown in blue squares, MTs are shown as thick horizontal lines, and the position of the left and right spindle pole is marked by the left and right edge of the thick lines linked to the left and right sister KTs, respectively. The average position of the pole-proximal end of the Ndc80 complexes on each (attached) kMT is shown in red and green discs for the left and right sister KTs, respectively. Growing and shrinking MTs are shown in green and yellow thick lines, respectively, for the left sister KT, and in red and magenta, respectively, for the right sister KT. Only the MTs to which at least one Ndc80 complex is bound are shown; therefore, the disappearance or appearance of the thick horizontal lines illustrates the dynamics of the full detachment and de novo binding of MTs, respectively.

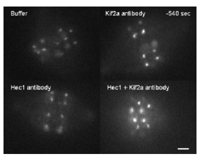

Video 2. **KT oscillation and inter-KT distance in HEC1-GFP PtK1 cells after Kif2a and Hec1 antibody microinjection.** Representative time-lapse movies of HEC1-GFP PtK1 cells microinjected as indicated in the labels. Images at a single focal plane were acquired by epifluorescence microscopy with an inverted microscope (Eclipse Ti; Nikon) using a fluorescence illumination system (Lumen 200PRO; Prior Scientific). Images were acquired at 20-s intervals and are played back at 7 frames per second. The videos start 10 min before anaphase onset, and stop with the first frame of anaphase. Note that the cell injected with anti-Hec1 antibody displays little/no KT oscillation (as evident from the dynamics of the GFP-labeled KTs). Moreover, the anti-Hec1–injected cell displays large inter-KT distances (the distance between Hec1-GFP marks on sister KTs), which are reduced by coinjection of anti-Kif2a antibody. Bar, 2 µm.

Table S1. **Model parameters**

Symbol	Description	[Range tested] (value used for figures)	Reference
Molecule number and structure-dependent parameters			
N	Maximal number of MT attachment sites at KT	[10–60] (30)	VandenBeldt et al., 2006
n_{Ndc80}	Number of Ndc80 complex per kMT	[8–15] (13)	Johnston et al., 2010
$N_{sliding}$	Number of sliding motor per kMT	[3–10] (4)	Assumed in this study
Mechanical and biophysical properties			
d_0^{coh} / d_0^{Ndc}	Rest length of cohesion bonds/Ndc80 complex	1.5 μm/100 nm	This study, Wan et al., 2012
$\kappa_{coh}/\kappa_{Ndc80}$	Spring constant of cohesion bonds/Ndc80 complex	[5–500] pNμm^{-1} (50/50)	Assumed in this study
$\varepsilon_{coh}/\varepsilon_{Ndc80}$	Viscous friction constant of cohesion bonds/Ndc80 complex	[5–100] pNsμm^{-1} (50/500)	Assumed in this study
μ_{chr}	Viscous drag coefficient of chromosome	[1–100] pNsμm^{-1} (10)	Estimated based on Marshall et al., 2001
$V_{sliding}^{max}$	Unloaded velocity of sliding/flux motors	[0.5–2] μm min^{-1} (1)	Estimated based on Cameron et al., 2006
$F_{sliding}^{stall}$	Stall force of sliding/flux motors	[0.1–10] pN (4)	Valentine et al., 2006
$F_{sliding}^{detach}$	Detachment force of sliding/flux motors	[0.1–10] pN (2)	Valentine et al., 2006
F_{poly}^{Ndc}	Ndc80 critical force for increase in detachment rate from polymerizing MT	[0.1–10] pN (0.1)	Assumed in this study
F_{depoly}^{Ndc}	Ndc80 critical force for decrease in detachment rate from depolymerizing MT	[−10–0.01] pN (−0.1)	Assumed in this study
F_{switch}	Ndc80 critical force for turnaround (increase) for detachment from depolymerizing MT	[0.1–20] pN (5)	Assumed in this study
F_{PE}^{max}	Constant PEF magnitude near spindle poles	[5–200] pN (30)	Assumed in this study
α	PEF exponent	[0.5–5] (1 and 4)	Ke et al., 2009
MT DI, sliding motor, and Ndc80 complex kinetic parameters			
v_g, v_s	MT plus end growth/shrinkage rate	[5–15] μm min^{-1} (8/10)	Estimated from Waters et al., 1996
k_{vg}, k_{vs}	Factor for MT plus end growth/shrinkage decrease when interacting with KT	[1–10] (3)	Assumed in this study
f_{cat}^0 , f_{res}^0	MT plus end "free" rescue/catastrophe rate	[0.1–3] min^{-1} (1.2/0.6)	Estimated from fit to PAF (Cimini et al., 2006)
L_{av}	MT length at which catastrophe rate is = f_{cat}^0	[2–6] μm (3)	Estimated from McDonald et al., 1992
V_g	Critical MT plus end polymerization rate for increase in catastrophe rate	[0.5–1] μm min^{-1} (0.9)	Estimated from Janson et al., 2003
F_{res}	Tension on MT plus end for e-fold increase in rescue rate	[5–50] pN (20)	Assumed in this study
$k_{on}^{sliding}$	First order MT binding rate of sliding/flux motor	[0.01–1] s^{-1} (0.6)	Assumed in this study
$k_{off}^{sliding}$	Detachment rate of sliding/flux motor from MT in the absence of force	[0.01–1] s^{-1} (0.2)	Assumed in this study
k_{on}^{Ndc80}	First order MT binding rate of Ndc80 complex	[0.01–0.5] s^{-1} (0.1)	Assumed in this study
$k_{off,poly}^{Ndc80}(0)$ $k_{off,depoly}^{Ndc80}(0)$	Detachment rate of Ndc80 complex from polymerizing/depolymerizing MT in the absence of force	[0.005–0.5] s^{-1} (0.3/0.01)	Assumed in this study

References

Cameron, L.A., G. Yang, D. Cimini, J.C. Canman, O. Kisurina-Evgenieva, A. Khodjakov, G. Danuser, and E.D. Salmon. 2006. Kinesin 5-independent poleward flux of kinetochore microtubules in PtK1 cells. *J. Cell Biol.* 173:173–179. http://dx.doi.org/10.1083/jcb.200601075

Cimini, D., X. Wan, C.B. Hirel, and E.D. Salmon. 2006. Aurora kinase promotes turnover of kinetochore microtubules to reduce chromosome segregation errors. *Curr. Biol.* 16:1711–1718. http://dx.doi.org/10.1016/j.cub.2006.07.022

Janson, M.E., M.E. de Dood, and M. Dogterom. 2003. Dynamic instability of microtubules is regulated by force. *J. Cell Biol.* 161:1029–1034. http://dx.doi.org/10.1083/jcb.200301147

Johnston, K., A. Joglekar, T. Hori, A. Suzuki, T. Fukagawa, and E.D. Salmon. 2010. Vertebrate kinetochore protein architecture: protein copy number. *J. Cell Biol.* 189:937–943. http://dx.doi.org/10.1083/jcb.200912022

Ke, K., J. Cheng, and A.J. Hunt. 2009. The distribution of polar ejection forces determines the amplitude of chromosome directional instability. *Curr. Biol.* 19:807–815. http://dx.doi.org/10.1016/j.cub.2009.04.036

Marshall, W.F., J.F. Marko, D.A. Agard, and J.W. Sedat. 2001. Chromosome elasticity and mitotic polar ejection force measured in living Drosophila embryos by four-dimensional microscopy-based motion analysis. *Curr. Biol.* 11:569–578. http://dx.doi.org/10.1016/S0960-9822(01)00180-4

McDonald, K.L., E.T. O'Toole, D.N. Mastronarde, and J.R. McIntosh. 1992. Kinetochore microtubules in PTK cells. *J. Cell Biol.* 118:369–383. http://dx.doi.org/10.1083/jcb.118.2.369

Valentine, M.T., P.M. Fordyce, T.C. Krzysiak, S.P. Gilbert, and S.M. Block. 2006. Individual dimers of the mitotic kinesin motor Eg5 step processively and support substantial loads in vitro. *Nat. Cell Biol.* 8:470–476. http://dx.doi.org/10.1038/ncb1394

VandenBeldt, K.J., R.M. Barnard, P.J. Hergert, X. Meng, H. Maiato, and B.F. McEwen. 2006. Kinetochores use a novel mechanism for coordinating the dynamics of individual microtubules. *Curr. Biol.* 16:1217–1223. http://dx.doi.org/10.1016/j.cub.2006.04.046

Wan, X., D. Cimini, L.A. Cameron, and E.D. Salmon. 2012. The coupling between sister kinetochore directional instability and oscillations in centromere stretch in metaphase PtK1 cells. *Mol. Biol. Cell*. 23:1035–1046. http://dx.doi.org/10.1091/mbc.E11-09-0767

Waters, J.C., T.J. Mitchison, C.L. Rieder, and E.D. Salmon. 1996. The kinetochore microtubule minus-end disassembly associated with poleward flux produces a force that can do work. *Mol. Biol. Cell*. 7:1547–1558.